Impact Craters in Granular Media: Grains against Grains

F. Pacheco-Vázquez and J. C. Ruiz-Suárez

CINVESTAV-Monterrey, PIIT Autopista Nueva al Aeropuerto Km. 9.5, Apodaca, Nuevo León 66600, México

(Received 26 August 2011; published 14 November 2011)

Impact experiments in granular media are usually performed with solid projectiles that do not fragment at all. Contrastingly, we study here the morphology produced by the impact of spherical granular projectiles whose structure is utterly lost after collision. Simple and complex craters are observed, depending on the packing fraction of the balls. Their diameters D and depths z are analyzed as a function of the drop height h. We find the same power law $D \propto h^{1/4}$ obtained with solid spheres, but a discontinuity at a certain threshold height, related to the cohesive energy of the projectiles, shows up. Counterintuitively, instead of a monotonic increase with the collisional energy, z becomes constant above this threshold.

DOI: 10.1103/PhysRevLett.107.218001 PACS numbers: 45.70.−n, 83.80.Fg

Years after Galileo turned his refracting telescope towards the Moon in 1609, observing for the first time circular depressions on its surface [1], geologists and astronomers proposed different hypotheses to explain the origin of lunar and planetary craters. Although impact theories [2,3] and other exotic conceptions like steam explosions [4] or coral atolls [5] were conceived, the dominating idea for 300 years was that craters had a volcanic origin [6–8]. Impact theory was revived at the beginning of the last century with the study of terrestrial craters [9,10] but not fully accepted until the 1960s [11]. Since then, many experiments and theoretical studies have been performed aiming to explain the observed morphologies and to find the relationships between the crater diameter D and its depth z with the impact energy E_k [12–15].

The simplest way to perform impact experiments is by releasing balls from a finite height into granular targets. Fortunately, although such low-speed impacts hardly reproduce the conditions that could have existed in past astronomic events, the information one can gather is not at all meaningless. Indeed, many interesting crater features have been reproduced [14] and crucial relationships found [13–15]. For instance, it has been discovered that $D \propto h^{1/4}$ [13] (h, the drop height, is proportional to E_k). Furthermore, it was found that $z \propto h^{1/3}$ [13,15], although an exponent of $1/4$ has also been reported [16]. It is important to remark that in all these low-speed impact experiments the projectiles used were unbreakable solid balls. However, real asteroids have a dominating granular structure (as revealed by their high porosity [17,18]) and disintegrate after collision. So, this raises an interesting question: Are the crater morphologies produced by solid and granular projectiles similar and described by the same relationships?

Aiming to answer the above question, we report in this Letter impact cratering experiments using granular projectiles with different packing fractions. We observed that if E_k is large enough to overcome the cohesion between the grains conforming the balls, they fragment and spread over the surface, resulting in crater morphologies that resemble those observed in moons and planets. At low packings, the impacts produce bowl-shaped simple craters; at higher packings, central peaks emerge. Above the cohesive energy, granular balls create larger craters than solid do, and crater depths are independent of E_k.

Our granular projectiles were prepared as follows: 150 ml ($\sim$ 260 g) of gray sand ($\rho_{gs} = 2.72$ g/cm3) and 15 ml of water are thoroughly mixed until a homogeneous mud is obtained. Approximately 35 ml of this material is put inside metal spherical shells that, once joined one against the other, form a consolidated (yet fragile) ball with diameter $d = 3.65 \pm 0.03$ cm. By changing the mass of the wet sand used and the pressure exerted, balls with five different packing fractions η and the same diameter are obtained. The balls were dried in an oven at 140 °C for 2 h and, after that, weighed by using an analytical balance. The dried balls can be grabbed with the fingers as if they were normal solid balls. The projectiles were carefully classified in five groups as a function of mass: $m = 33$, 37, 41, 44.4, and 45.5, ± 0.5 g corresponding to $\eta = 0.48$, 0.54, 0.60, 0.64, and 0.66, ± 0.01, respectively; see Supplemental Material, Fig. 1(a).

Let us now describe a typical impact experiment. First, we prepare the granular target: A cylinder of 45 cm diameter and 30 cm high is overfilled with white sand ($\rho_{ws} = 2.65$ g/cm^3), and it is randomized by mixing the medium with a rotating comb of thin steel rods inserted into it. The comb is removed, and the material that exceeds the height of the cylinder is swept with a horizontal bar, obtaining a flat surface. The packing fraction produced by this method is $\eta_{ws} = 0.55 \pm 0.01$. Next, we place a granular projectile in an electromechanical gate at a given height h measured from the surface of the sand bed. The gate is opened, and the projectile falls vertically, impacting on the center of the target. A wide interval of heights was investigated, ranging from 5 up to 1350 cm, corresponding to impact velocities ($v = \sqrt{2gh}$) in the range of

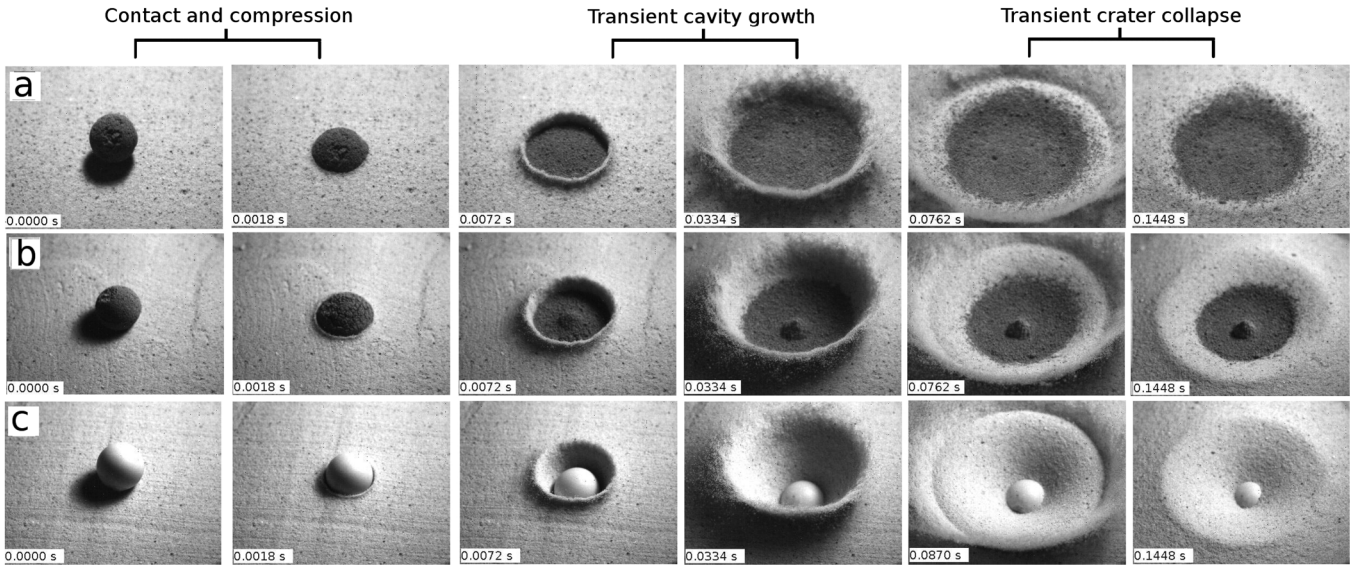

FIG. 1. Impact crater formation process: (a) a granular projectile with $\eta = 0.54$ ($m = 37$ g), (b) a granular projectile with $\eta = 0.66$ ($m = 45.5$ g), and (c) a solid projectile ($m = 45.5$ g). In all three cases $h = 640$ cm and $d = 3.65$ cm. Low-packed projectiles produce simple shallow craters with a thin layer of the projectile material covering it. High-packed ones produce deeper craters and central peaks surrounded by the sprayed material, which resemble Thyco's morphology in our Moon.

10^2–10^5 cm/s and energies E_k from 10^5 to 10^{11} erg. The granular projectiles create well-defined craters, but depending on the value of these energies—low, intermediate, and high—they do not fragment at all (displaying the same impact dynamics shown by solid ones), fragment, or fully pulverize, respectively. In our experiments, the inverse Froude number $\mathrm{Fr}^{-1} = gd/2v^2$ (the ratio of gravitational to dynamic pressures [16]) takes values from 10^{-4} to 0.18, which overlap with the corresponding values achieved in planetary impact craters, where $10^{-6} < \mathrm{Fr}^{-1} < 10^{-2}$ [12].

Figure 1 shows a sequence of three different impact events taken by a high speed camera (DRS Lightning RDT Plus) at 5000 fps: (a) a loose-packed granular projectile ($m = 37$ g) generating a simple crater (Movie 1) [19], (b) a high-packed granular projectile ($m = 45.5$ g) producing a central peak (Movie 2) [19], and (c) the impact of a solid projectile ($m = 45.5$ g), for comparison reasons. The sequence was divided in three different stages [20]: contact and compression, from impact until fragmentation; transient cavity growth, from fragmentation until the projectile material is deposited on the granular bed; and the crater collapse. Even when each one of these stages takes approximately the same time, the final distribution of the material is notably different.

Figure 2(a) shows top views for all the crater morphologies observed in our experiments, and their dependence in terms of η and h are displayed in Fig. 2(b). If h is small, the projectiles do not fragment with the impact (blue circles). However, as h is increased, fragmentation is seen at $h \approx h_f$ ($\oplus$) that augments with the packing of the ball (the threshold energy E_c, that naturally depends on its porosity, is proportional to h_f). A loose-packed projectile easily breaks when it is released at a short distance from the surface, but h_f rapidly increases up to $h \sim 150$ cm for the highest packing studied. Slightly above h_f, lumps are spread over the crater ($\circledast$). For $h \gg h_f$, the morphology depends basically on the packing. Orange circles represent simple craters, typical of projectiles with $\eta \lesssim 0.60$. For $0.60 \lesssim \eta \lesssim 0.66$, a small peak starts to show up ($\odot$), revealing a transition from simple to complex crater formation. Finally, peaks are always formed for $\eta \gtrsim 0.66$ (circled solid black circles).

Whereas the simple crater formation in Fig. 1(a) is expected, the appearance of the central peak is not. A possible mechanism is the emergence of a granular jet, as those observed with steel balls impacting loose sand [16,21]. Along this direction, studies have been carefully pursued to explain the appearance of such complex craters based on a nonlinear mechanism produced by a possible restructuring of the melted surface [20]. However, high speed videos in our experiments, where emerging jets never appear, rule out this possibility; see Movie 2 [19]. A second mechanism can be related to an insufficient kinetic energy, unable to surpass the cohesive forces of the projectile that could leave a portion intact. To test it, we quadruplicated the impact energy by releasing balls of 45.5 g from a tall tower of $h = 1350$ cm. The peaks keep forming and are much better defined [Fig. 2(c)], discarding this second possibility. To determine the effect of the mass, we dropped a heavier projectile: $m = 124$ g and $d = 5.1$ cm, with the same $\eta = 0.66 \pm 0.01$. We obtained larger craters and also a central peak; see Fig. 2(d). When the packing of these heavy balls was reduced to $\eta = 0.60$, the peaks disappear and simple

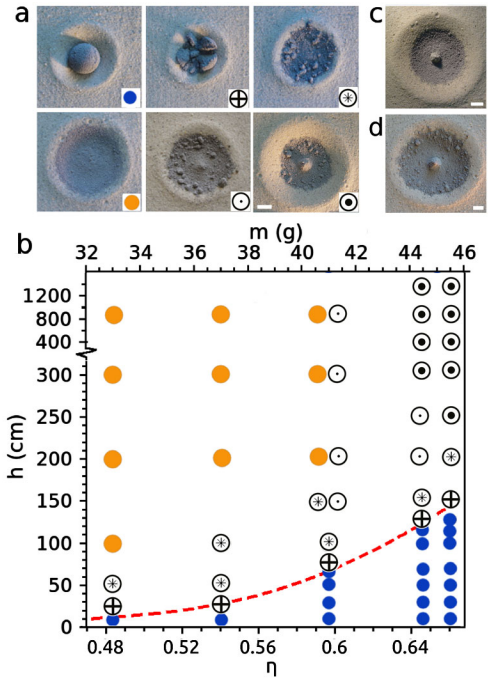

FIG. 2 (color online). (a) Different morphologies obtained in our experiments using granular projectiles of $d = 3.65$ cm. Simple (orange circles) and complex (circled solid black circles) craters are produced at $h = 300$ cm for $\eta = 0.54$ and 0.66, respectively (scale bar = 2 cm). (b) A phase diagram $h - \eta$, where the symbols are in correspondence with (a). The red line corresponds to the fragmentation height; see Supplemental Material, Fig. 1 [22]. Even when the kinetic energy is dramatically increased, by changing the impact velocity or the mass, the central peak formation appears: (c) complex crater obtained for $h = 1350$ cm, $\eta = 0.66$, $m = 45.5$ g, and $d = 3.65$ cm and (d) complex crater obtained for $h = 300$ cm, $\eta = 0.66$, $m = 124$ g, and $d = 5.1$ cm.

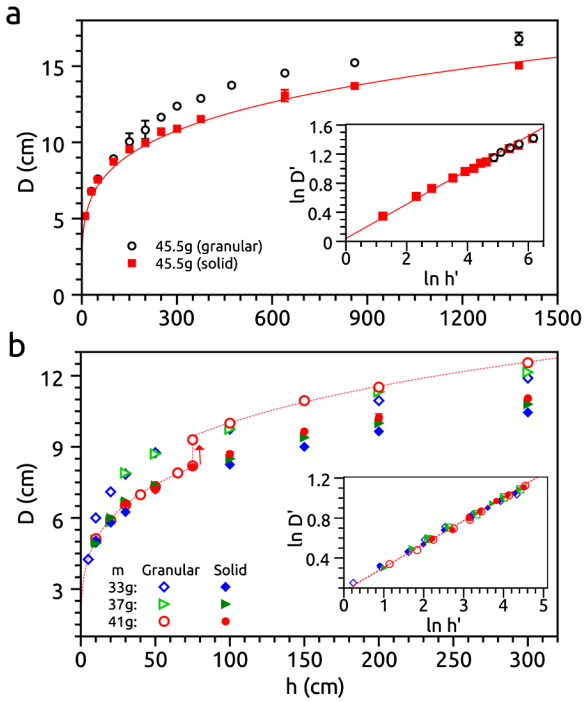

FIG. 3 (color online). (a) D vs h for granular projectiles of $\eta = 0.66$ (○) and solid projectiles with the same values of m and d (red squares). For $h < h_f$ the craters produced by both projectiles have the same diameter, but they start to be greater for the granular case until the difference ΔD reaches a constant value. (b) Similar behaviors are obtained for $\eta = 0.48$ (blue diamonds), 0.54 (green triangles), and 0.60 (orange circles), but the gap between diameters appears more abruptly. The red solid lines in (a) and (b) are obtained from Eq. (1), by using $m = 45.5$ and 41 g, for solid and granular projectiles, respectively, and $C = 2.87$.

craters form again. Thus it seems that the key factor is not the mass but the packing, which gives us a hint of the mechanism working here.

Snapshots in Fig. 1(b) show that the peak starts to appear just after the impact, and the high speed video (Movie 2) [19] reveals that the upper material of the granular projectile slides as an ultrafast avalanche over a granular pile formed initially. So, we claim that the mechanism in the peak formation is the following: For low-packed projectiles, the high porosity enables its internal material to rearrange and fully spray during the impact. An initial pile is not formed. On the other hand, the high packing avoids this internal rearrangement, and the pile is produced by a dynamic confinement during the transient cavity growth. This mechanism is illustrated by impacting a ball with two different color hemispheres onto solid and granular surfaces, where it is clear that the lower hemisphere produces the pile; see Movie 3 [19] and Supplemental Material, Fig. 2 [22].

Now, we compare D vs h for solid and granular projectiles of the same diameter ($d = 3.65$ cm). In Fig. 3(a), we show the results for $m = 45.5$ g. Before fragmentation, D is equal for both cases, but discrepancies start to appear when $h = h_f \approx 150$ cm. Then, the crater produced by a granular projectile grows faster than that produced by the solid one. After $h = 380$ cm, the difference ΔD remains constant in all the interval. The same gap is observed for $\eta = 0.48$, 0.54, and 0.60 in Fig. 3(b), but for these packings the transitions appear abruptly in $h_f = 10$, 30, and 75, ± 5 cm, respectively. So, the smooth transition in Fig. 3(a) can be related to the pile formation process due to the fact that the material is not fully spread in the crater (i.e., the dynamics is a combination of those produced by solid and granular projectiles).

It is intriguing that in all these cases $\Delta D = 1.31 \pm 0.03$ cm, independently of m and h (Supplemental Material, Fig. 3 [22]). The same behavior is observed for balls of $d = 5.1$ cm, although in this case $\Delta D = 2.28 \pm 0.16$ cm (Supplemental Material, Fig. 4 [22]). Then, ΔD is a shape factor that depends on the diameter of the projectile.

For low-speed impacts of solids balls impacting on different granular materials, it has been found by Uehara

et al. [13] that $D \propto (\rho_b/\rho_t)^{\alpha} d^{1-\alpha} h^{\alpha}$ with $\alpha = 0.231 \pm 0.005$. We have used a similar power law to fit our data, plus an extra term that includes ΔD for $h \geq h_f$ for granular events. The insets in Figs. 3(a) and 3(b) show that all data collapse in a log-log plot of D' vs h' with $D' = [D - \Theta(h - h_f)\Delta D]/d$ and $h' = (\rho_b/\rho_t)h/d$, where $\rho_b = \eta\rho_{gs}$ and $\rho_t = \eta_{ws}\rho_{ws}$. The exponent for the power-law fit is 0.235 ± 0.006, similar to that obtained in Ref. [13]. Hence, the craters produced by solid and granular projectiles follow the same power-law dependence, but it is necessary to consider a discontinuity that appears after fragmentation. Thus, the crater diameters, regardless the nature of the projectile, are given by

$$D = C\left(\frac{\rho_b}{\rho_t}\right)^{1/4} d^{3/4} h^{1/4} + (\Delta D)\Theta(h - h_f), \qquad (1)$$

where $\Theta(h - h_f)$ is the Heaviside step function. The above equation suggests that in the granular case there is a higher vertical-to-horizontal momentum transfer during the impact. A similar momentum transference has been observed before when a jet of dry beads impacts into a granular bed [23].

Finally, we consider z as a function of h. For impacts of solid projectiles, the final depth was measured from the initial surface to the bottom of the ball. For granular projectiles, this measurement was taken by a vertical cut at the middle of the crater (similarly to slicing a cake) using a thin transparent glass of $30 \times 30 \times 0.01$ cm (length, height, and width) as shown in the left image in Fig. 4(a). This method allows us to have a lateral view of the material distribution to find the final depth (due to the contrast between the color of the two kinds of sand). A frontal picture was taken and analyzed by using IMAGEJ. Because of the thickness of the glass, a little quantity of gray sand is dragged 0.5 ± 0.2 cm. We consider this effect by subtracting it from the experimental measurements. The same results are found if carefully removing the gray sand inside the crater until reaching the white sand at the bottom of the crater (right image). Figure 4(a) shows z vs h for $m = 45.5$ g. For $h < h_f$ both solid and granular projectiles reach the same final depth, but at $h = h_f$ the granular projectile breaks and penetrates notably less. Here, an unexpected behavior appears: For $h > h_f$ the value of z remains constant in all the studied range, in contrast to what is observed for solid projectiles, where the depth depends on the impact energy. The same behavior is observed for other values of m in Fig. 4(b), where z decreases for less-packed projectiles, supporting our previous argument that a vertical-to-horizontal momentum transfer is produced.

In conclusion, we carried out impact cratering experiments using granular projectiles with different porosities. While some similarities are found with crater morphologies produced by solid balls, granular ones give rise to unexpected behaviors: (i) Bowl-shaped craters with or without central peaks are produced depending on the packing, (ii) even when their diameters follow the same power-law dependence, craters produced by granular projectiles are larger that those produced by equivalent solid balls, and (iii) final depths are constant above a given drop height. We believe our results may give new clues to understand the physical mechanism involved in natural crater formation.

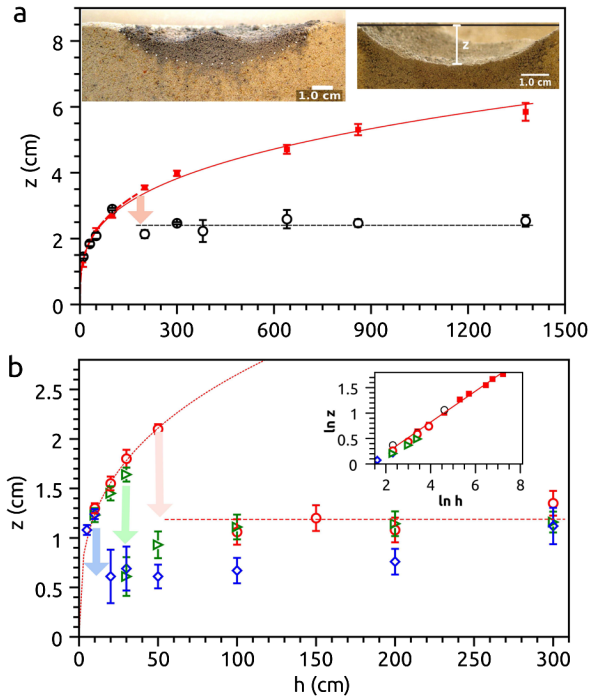

FIG. 4 (color online). Final penetration depth z vs h for different packing fractions. (a) Solid projectiles (red squares) obey a power-law dependence with exponent 0.304 ± 0.007 [which is the slope of the red line shown in the inset in (b)]. This exponent is similar to the value found in Ref. [13]. On the other hand, granular projectiles (○) follow the same dependence until $h = h_f$. At this value, z decreases abruptly and remains constant in all the interval studied ($150 < h < 1350$ cm). (b) The same constant depth is observed for other values of η. The images in (a) show two different methods used to obtain z for granular impacts (see the text). Symbols are in correspondence with Fig. 3.

This work has been supported by Conacyt, Mexico, under Grant No. 101384.

[1] C. Koeberl, Earth Moon Planets **85**, 209 (2001).
[2] R. Hooke, *Micrographia* (Dover, New York, 1961).
[3] R. A. Proctor, in *The Moon: Her Motions, Aspect, Scenery, and Physical Condition* (Alfred Brothers, Manchester, 1873).
[4] W. H. Pickering, *The Moon* (Doubleday, New York, 1903), p. 103.
[5] D. P. Beard, Popular Astron. **33**, 74 (1925).
[6] J. Nasmyth and J. Carpenter, in *The Moon: Considered as a Planet, a World, and a Satellite* (John Murray, London, 1874), p. 189.

[7] W. W. Campbell, Publ. Astron. Soc. Pac. **32**, 126 (1920).
[8] G. E. Hale, Publ. Astron. Soc. Pac. **32**, 112 (1920).
[9] E. Opik, Bull. Soc. Russe Amis Etude Univers **3**, 125 (1916).
[10] A. Wegener, The Moon **14**, 211 (1975) (translated by A. M. Celal Sengor).
[11] For a brief history of the craters origin hypothesis, see [1] and the references therein.
[12] K. A. Holsapple, Annu. Rev. Earth Planet. Sci. **21**, 333 (1993).
[13] J. S. Uehara, M. A. Ambroso, R. P. Ojha, and D. J. Durian, Phys. Rev. Lett. **90**, 194301 (2003).
[14] J. R. de Bruyn and A. M. Walsh, Can. J. Phys. **82**, 439 (2004).
[15] M. A. Ambroso *et al.*, Phys. Rev. E **71**, 051305 (2005).
[16] A. Q. Walsh, K. E. Holloway, P. Habdas, and J. R. de Bruyn, Phys. Rev. Lett. **91**, 104301 (2003).
[17] D. T. Britt *et al.*, *Asteroids III* (University of Arizona, Tucson, 2002), pp. 485–500.
[18] D. J. Scheeres, C. M. Hartzell, P. Sanchez, and M. Swift, Icarus **210**, 968 (2010).
[19] See Supplemental Material at http://link.aps.org/supplemental/10.1103/PhysRevLett.107.218001 for movies of the impact of granular projectiles.
[20] H. J. Melosh and B. A. Ivanov, Annu. Rev. Earth Planet. Sci. **27**, 385 (1999).
[21] D. Lohse *et al.*, Phys. Rev. Lett. **93**, 198003 (2004).
[22] See Supplemental Material at http://link.aps.org/supplemental/10.1103/PhysRevLett.107.218001 for supplemental information.
[23] F. Pacheco-Vázquez and J. C. Ruiz-Suárez, Nature Commun. **1**, 123 (2010).